

NANO EXPRESS

Open Access



Improvement in the photoelectric conversion efficiency for the flexible fibrous dye-sensitized solar cells

Gentian Yue^{1,2*}, Xianqing Liu^{1,2}, Ying Chen², Jinghao Huo³ and Haiwu Zheng^{1,2*}

Abstract

A dye-sensitized and flexible TiO₂ fiber with multilayer structure was prepared by using brush method as the photoanode in the efficient flexible fibrous dye-sensitized solar cells (FFDSSCs) to avoid electronic recombination and improve the electronic capture efficiency. The composite Pt counter electrode, preparation from the surface modification of the electrodeposited Pt wire by using a simple one-step thermal decomposition approach of H₂PtCl₆ isopropanol and n-butyl alcohol (volume ratio = 1:1) solution, provided a significant improvement in electrocatalytic activity, which was confirmed by extensive electrochemical tests. The FFDSSC assembled with the fiber-shaped TiO₂ photoanode and the composite Pt counter electrode achieves an enhanced photoelectric conversion efficiency of 6.35%, higher than that of the FFDSSC with monolayer fibrous TiO₂ photoanode and electrodeposited Pt wire counter electrode. More importantly, the photoelectric conversion efficiency of 6.35% is comparable to that of the FFDSSC based on the pure Pt wire counter electrode (6.32%). The FFDSSC with high elasticity, flexibility, and stretchability can adapt to complex mechanical deformations, which is of great significance for the development of wearable electronics in the future.

Keywords: Flexible, Multilayer, Fibrous, Dye-sensitized solar cell

Background

Dye-sensitized solar cells (DSSCs) are regarded as one of the most promising next-generation photovoltaic cells to replace conventional Si-based solar cells for their advantages of low-cost, high power conversion efficiency, and environmental friendliness [1, 2]. However, the solar cells with the rigid conductive glass are now facing limitations in practical application such as transportation, installation, handling, and smart textile systems [3–5]. To overcome such issues and to broaden its application area, fiber-shaped solar cells as a promising candidate for future applications with various directions are extensively concerned by DSSC researchers.

Fibrous solar cells exhibit unique advantages of being lightweight, wearable, and adaptive to a variety of curved surfaces like our bodies in comparison with planar photovoltaic devices and thus are robustly developing

to fulfill the demands of various wearable electronics in modern life [6–8]. In addition to the advantages of the flat plate flexible DSSC, fiber-like solar cells have unique advantage of three-dimensional lighting, which can make full use of diffuse light from all angles.

Several studies on fibrous DSSCs have been reported preparation with modified titanium wire as photoanode and pure platinum (Pt) wire as counter electrodes (CE) [9, 10]. Of course Pt is one of the most selective materials for catalyzing the reduction of I₃⁻ to I⁻ due to its superior electrocatalytic activity, stability, and excellent conductivity; however, it is very high-cost with pure Pt wire as CE and disfavors the scale-up production for fibrous devices. Therefore, effective design of electrode including low-cost CE with high conductivity and catalytic ability is essential. Many reports have discovered several options by thermal decomposition or electrochemical reduction to prepare the Pt films with the same function as pure platinum, which significantly reduces the usage amount of platinum [11–14]. In addition, the performance of the FFDSSC with modified titanium wire photoanode is low due to its small

* Correspondence: yuegentian@126.com; zhenghaiw@ustc.edu

¹Henan Key Laboratory of Photovoltaic Materials, Henan University, Kaifeng 475004, China

Full list of author information is available at the end of the article

loading of dye and electron recombination. Many attempts are made to enhance the efficiency of the optical absorption and charge transport by surface modification, particle size changing, and multi-structure construction for the photoanode. The main aim is to develop high-performance fiber electrodes in enhancing the photovoltaic performances of fiber-shaped solar cells.

Herein, a flexible fibrous DSSC (FFDSSC) based on a flexible fibrous TiO₂ photoanode with smooth surface coated on the Ti wire substrate by using a multi-step sintering method, and a modified Pt composite CE prepared with Al wire as inner core via a two-step electrochemical-thermal decomposition approach were envisaged to enhance the photo-electric conversion efficiency. As expected, the modified composite Pt CE showed excellent electrocatalytic activity and low charge transfer resistance of 3.11 Ω cm² through the extensive electrochemical measurements. The FFDSSC exhibited a considerably improved performance in photo-electric conversion efficiency of 6.35% under irradiation of 100 mW cm⁻² (AM 1.5).

Methods

Materials

The nickel (II) chloride hexahydrate (NiCl₂·6H₂O, 98%), thiourea (TU, ≥99.0%), cobalt chloride hexahydrate (CoCl₂·6H₂O, 98%), ethanol, chloroplatinic acid, titanium tetrachloride (TiCl₄), and tetra-n-butyl titanate are purchased from Shanghai Chemical Agent Ltd., China. All reagents are of analytical reagent grade. The aluminum and titanium wire (diameter = 0.2 mm, 99.999%) are purchased from Shengshida Metallic Material Co., Ltd. China. The organometallic compound sensitized dye N719 is obtained from Solaronix SA (Switzerland). The TiO₂ paste (diameter = 20 nm) are purchased from Wuhan Geao Co., Ltd. China.

Preparation of flexible fibrous TiO₂ photoanode

The aluminum and titanium wires with length of 15 cm were polished by sandpaper and ultrasonically cleaned sequentially in detergent, acetone, distilled water, and ethanol for 30 min, respectively, and then stored in isopropyl alcohol. The TiCl₄ solutions were configured with the concentration of 0.03 and 0.05 M and stored in refrigerator.

The dye-sensitized flexible fibrous TiO₂ photoanode was prepared referred to our previous reports [15–17]. Firstly, a barrier layer was formed by immersing the titanium wire substrate with length of 15 cm in 0.03 M TiCl₄ solution at 70 °C for 1 h, followed by sintering at 450 °C for 30 min in air. This process repeats five times to increase the loading of TiO₂. Subsequently, the TiO₂ layer with particle size of 20 nm was coated onto the barrier layer by using brush method and then sintered at

450 °C for 30 min in air. This process repeats three times to form a smooth surface. A modified layer is formed by immersing the abovementioned TiO₂ substrate in 0.05 M TiCl₄ solution at 70 °C for 1 h and sintering at 450 °C for another 30 min. This process repeats two times to make sure the TiO₂ pores are filled. The dye was loaded by immersing the fibrous TiO₂ anode in 0.3 mM of dye N719 Tert-butanol/acetonitrile solution for 12 h. Thus, the dye-sensitized flexible fibrous TiO₂ photoanode was obtained.

Preparation of Pt fibrous CE and fabrication of FFDSSCs

Fibrous Pt CE was prepared by a two-step electrochemical-thermal decomposition approach. Firstly, aluminum wire was soaked into 0.01 M H₂PtCl₆ and LiClO₄ ethanol solution to carry out the electrodeposition procedure and got Pt-1 fibrous CE. The obtained Pt-1 fibrous CE was heated to 250 °C, and then 0.5 ml of H₂PtCl₆ (1.0 wt%) isopropanol and n-butyl alcohol (volume ratio = 1:1) solution containing OP emulsification agent (1.0 wt%) was rapidly dropped onto the surface of the Pt-1 fibrous CE and sintered at 450 °C for 30 min to remove some residual organic compounds in the platinum layer, and a microporous platinum film thus was prepared and signed Pt-2 fibrous CE. The Pt-2 fibrous CE was twisted around the fibrous TiO₂ photoanode with approximately 0.5 mm pitch to form a flexible fiber-shaped DSSC (as shown in Fig. 1). The resulted wire was sealed into a plastic tube (diameter of 0.5 mm), and redox electrolyte (0.05 M of I₂, 0.1 M of LiI, 0.6 M of tetrabutylammonium iodide, and 0.5 M of TBP in acetonitrile) was injected with a syringe and sealed with the UV-cure adhesion (HT8803) to prevent from leakage or evaporation of liquid electrolyte. For comparison, the flexible fiber-shaped DSSCs (based on the Pt-1 and pure Pt CEs, and the fibrous TiO₂ photoanode with and without TiCl₄ modification) were prepared using a similar process.

Characterization

The surface morphologies of the samples were observed by using JSM-7001F field emission scanning electron microscope (SEM). Energy dispersive spectroscopy analysis (EDS) was obtained from Bruker-ASX (Model Quan-Tax 200). Cyclic voltammetry (CV) measurements were conducted in a three-electrode one-compartment cell, in which an as-prepared Pt wire was taken as the working electrode, a Pt sheet of 1.5 cm² as CE, and an Ag/AgCl electrode as reference electrode in an acetonitrile solution consisting of 10 mM LiI, 1 mM I₂, and 0.1 M LiClO₄. The EIS tests were carried out simulating open-circuit conditions at ambient atmosphere by using an electrochemical measurement system (CHI660E, Shanghai Chenhua Device Company, China) at a constant temperature of

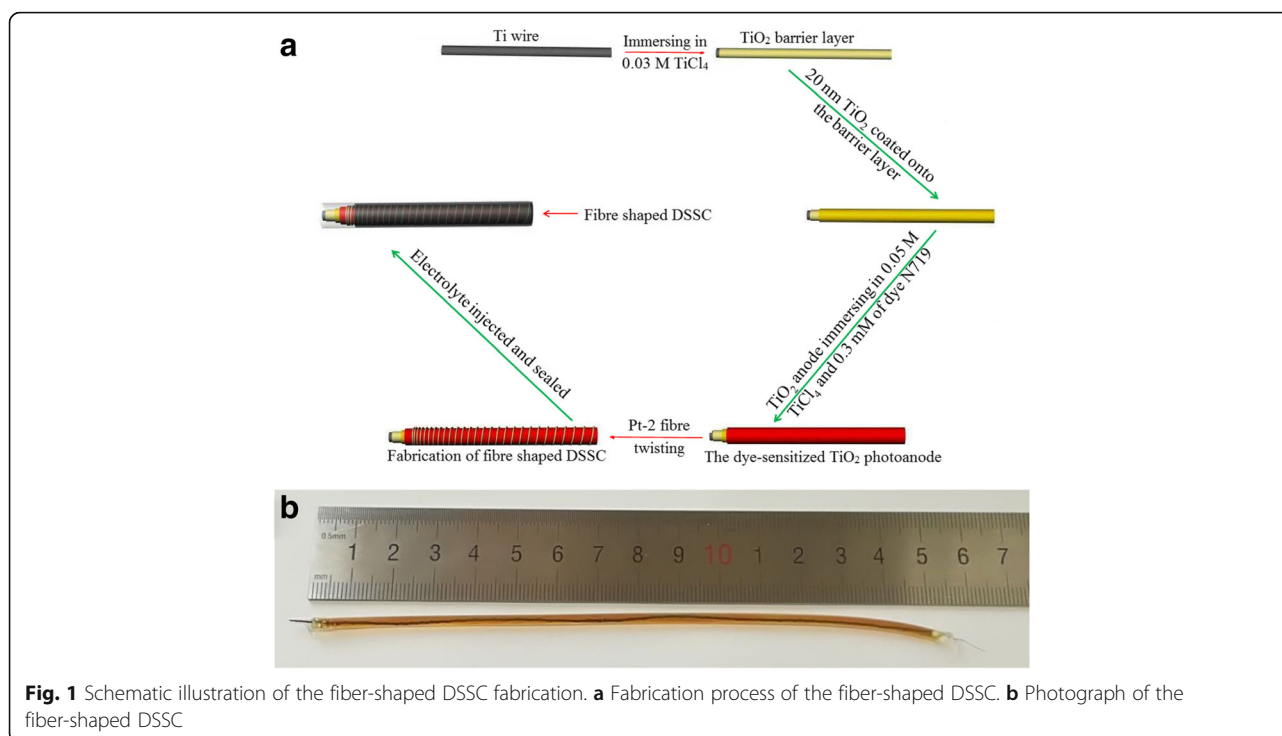


Fig. 1 Schematic illustration of the fiber-shaped DSSC fabrication. **a** Fabrication process of the fiber-shaped DSSC. **b** Photograph of the fiber-shaped DSSC

20 °C with AC signal amplitude of 20 mV in the frequency range from 0.1 to 10^5 Hz at 0 V DC bias in the dark.

The photovoltaic tests of FFDSSCs were carried out by measuring photocurrent-photovoltage (J - V) characteristic curves under irradiation of 100 mW cm^{-2} from the solar simulator (CEL-S500, Beijing China Education Au-light Co., Ltd) in ambient atmosphere. The fill factor (FF) and the photo-electric conversion efficiency (η) of DSSC were calculated according to the following equations:

$$\eta (\%) = \frac{V_{\text{max}} \times J_{\text{max}}}{P_{\text{in}}} \times 100\% = \frac{V_{\text{oc}} \times J_{\text{sc}} \times \text{FF}}{P_{\text{in}}} \times 100\% \quad (1)$$

$$\text{FF} = \frac{V_{\text{max}} \times J_{\text{max}}}{V_{\text{oc}} \times J_{\text{sc}}} \quad (2)$$

where J_{sc} is the short-circuit current density (mA cm^{-2}); V_{oc} is the open-circuit voltage (V), P_{in} is the incident light power (mW cm^{-2}) and J_{max} (mA cm^{-2}) and V_{max} (V) are the current density and voltage at the point of maximum power output in the J - V curve, respectively.

Results and discussion

Surface morphology and composition of the samples

Figure 2 presents the SEM images of the fiber-shaped TiO_2 photoanode and Pt CE with different resolutions, the EDS images of the fibrous Pt CE, and the TiO_2 photoanode before and after sensitizing. From Fig. 2a

and b, the fiber-shaped TiO_2 photoanode remains smooth surface and porous structure, and the TiO_2 nanoparticles disperse uniformly in the Ti wire. Thus, the fiber-shaped TiO_2 photoanode modified with TiCl_4 twice formed the TiO_2 barrier layer, which can effectively prevent the electron recombination between the electrolyte and Ti fiber. From Fig. 2c and d, it can be seen that the surface of the fibrous Pt CE is smooth, uniform micropores and few bulges, which came from the rapidly boiling and volatilizing of isopropanol, and a large amount of pores were in situ generated in the surface of the electrodeposition Pt. Such a surface morphology of the modified fiber-shaped Pt CE largely increases the specific surface area of platinum fiber and are availed for the adsorption of liquid electrolyte [18], consequently resulting in a great improvement of photocurrent density and open-circuit voltage for the FFDSSC. Figure 2e and f show the EDS images of the TiO_2 photoanodes before and after sensitizing, respectively. Compared to Fig. 2e, f reveals that the TiO_2 photoanode was successfully sensitized from the strong signal of Ru element. The strong signals for the Al and Pt elements as shown in Fig. 2g indicate that the fibrous Pt CE was prepared with Al wire as inner core.

Electrochemical properties

Figure 3 presents the cyclic voltammograms of the electrodeposition Pt CEs before and after modified with thermal decomposition Pt at the scan rate of 50 mV s^{-1} to investigate the electrocatalytic activity of the samples in the

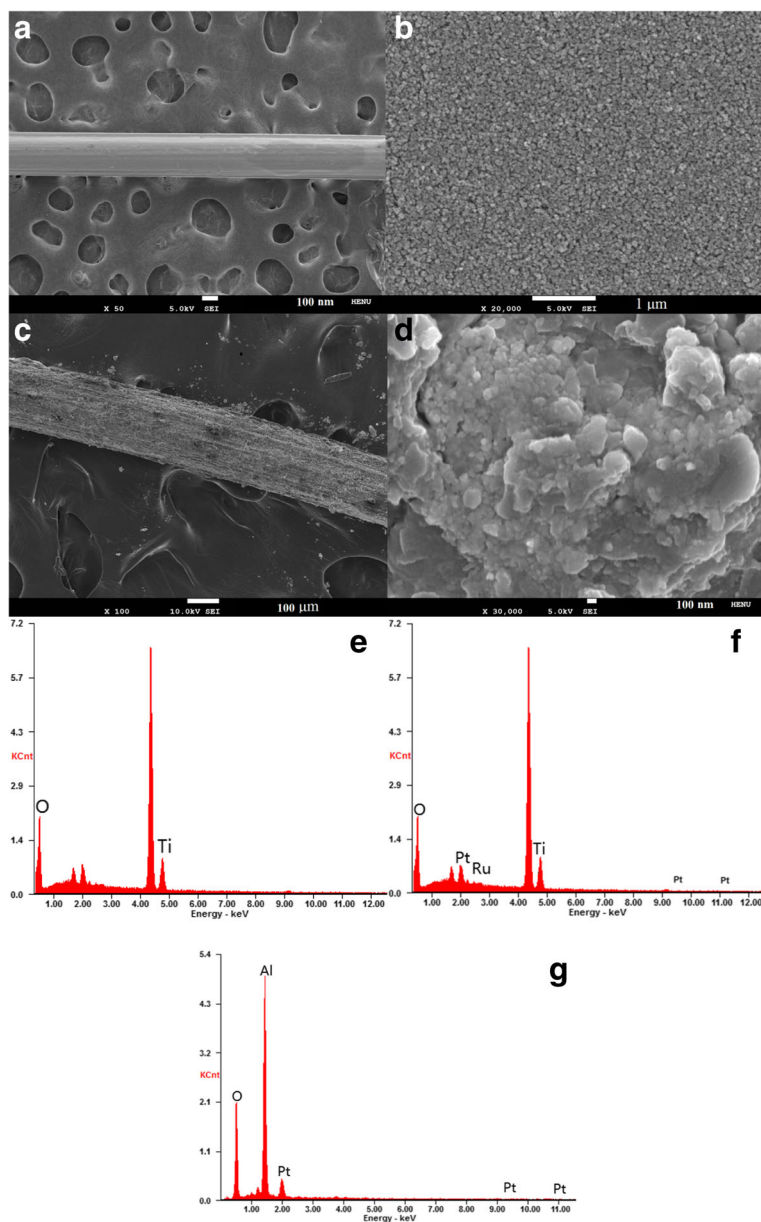


Fig. 2 The SEM images of the TiO₂ photoanode (a, b) and fibrous Pt CE (c, d) with different resolutions, the EDS images of the TiO₂ photoanode before (e) and after (f) sensitizing, and the fibrous Pt CE (g)

potential interval of -0.4 to 1.0 V. To our knowledge, the absolute value of cathodic peak current density $|I_{pc}|$ is positively correlated with the catalytic ability of electrodes, and the absolute value of peak-to-peak separation $|E_{pp}|$ is inversely correlated with the electrocatalytic activity of the CEs [19, 20]. Figure 3 gives almost identical shapes of two pairs of redox peaks and $|E_{pp}|$ for the Pt-1 and Pt-2 CEs in I^-/I_3^- redox system, and the $|I_{pc}|$ of the Pt-1 and Pt-2 CEs are 2.10 and 2.87 mA cm⁻², respectively, which exhibits much higher cathodic peak current density for the Pt-2 CE. This attributes to the large active surface area and

micropores structure of the Pt-2 CE made from the rapidly boiling and volatilizing of isopropanol, and a large amount of pores generated in situ in the platinum film. It was noticed that though the Pt-1 and Pt-2 CEs exhibit a similar $|E_{pp}|$, however, the Pt-2 CE shows much higher $|I_{pc}|$ than that of the Pt-1 CE. This indicates that the Pt-2 CE is more effectively acted as a catalyst in the reaction of the I^-/I_3^- electrolyte than that of the Pt-1 CE. More importantly, the Pt-2 CE with double-layer structure exhibits higher values for the $|I_{pc}|$ and $|E_{pp}|$ than that of the pure Pt fiber CE (listed in Table 1). The fact fully proves that the Pt-2 CE

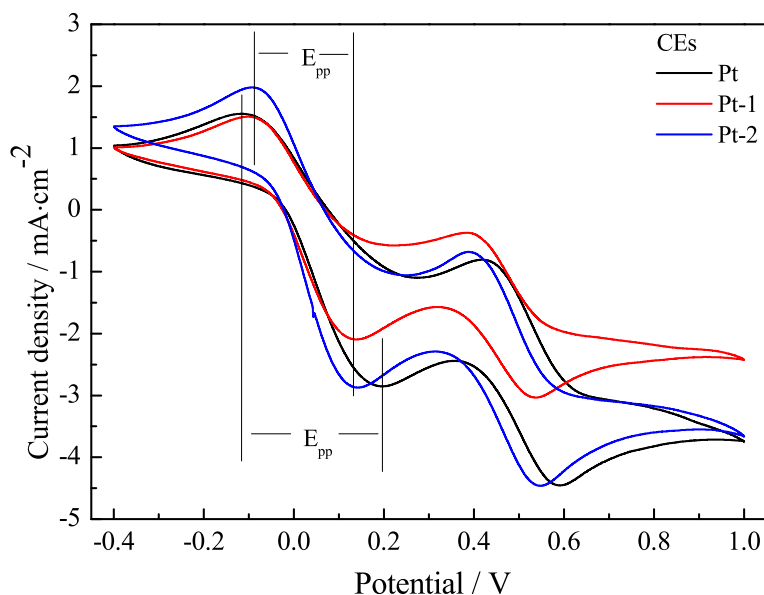


Fig. 3 The cyclic voltammograms for the Pt-1, Pt-2, and pure Pt CEs at the scan rate of 50 mV s^{-1}

with low-cost and simple preparation performs the same function as the pure Pt fiber CE. Consequently, the electrodeposition Pt CE modified with thermal decomposition Pt is an efficient electrocatalyst and has a good electrocatalytic ability for the I^-/I_3^- redox reaction.

Figure 4 shows 50 cycles cyclic voltammograms for the Pt-2 CE at the scan rate of 50 mV s^{-1} to investigate the long-term electrochemical stability of a CE. As presented in Fig. 4, the normalized cathodic and anodic peak current densities keep scarcely changed after being tested for 50 consecutive cycles. This suggests that the electrodeposition Pt CE after modified with H_2PtCl_6 thermal decomposition coated on the Al substrate possesses excellent electrochemical and chemical stability.

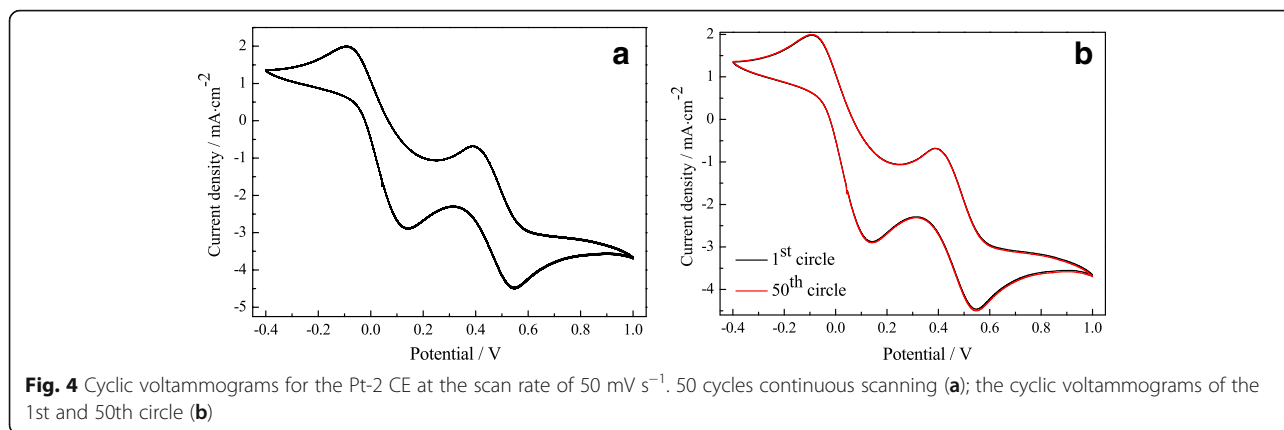
Electrochemical impedances of the CEs are effective and extensive tools to investigate the charge transport process. Figure 5 shows the Nyquist plots of the symmetrical Pt-1, Pt-2, and pure Pt CEs for I^-/I_3^- electrolyte, and the corresponding EIS parameters are also listed in Table 1, in which the R_s is the resistance value at the onset point of the first semicircle, the R_{ct} is the radius of the first semicircle, and the semicircle represents the Nernst diffusion impedance (Z_w) corresponding to the diffusion resistance of the I^-/I_3^- redox species [21, 22]. As is known to all, the R_{ct} is a crucial parameter for comparing the

electrocatalytic ability of different CEs, which is inversely correlated with the catalytic ability of the CEs. From Fig. 5 and Table 1, the R_s associated with the Pt-1, Pt-2, and pure Pt CEs are 3.96, 3.57, and $3.75 \Omega\text{-cm}^2$, respectively. The R_{ct} for the Pt-1, Pt-2, and pure Pt CEs are 3.99, 3.11, and $3.10 \Omega\text{ cm}^{-2}$, respectively. In other words, the R_s and R_{ct} for the abovementioned CEs follow the orders of Pt-1 > Pt-2 > Pt. Thus, it is comparable to that of the Pt-1 CE and indicates a lower interfacial charge transfer resistance occurred at the interface between the Pt-2 CE and I^-/I_3^- electrolyte under the same testing conditions. These results fully prove that the Pt-2 CE with double-layer structure after thermal decomposition Pt modifying shows great improvement in electrochemical catalytic ability compared to the pure Pt CE. The reasons for enhancing the performance of the CE can be attributed to the surface structure, i.e., uniform micropores and few bulges, and good electrochemical properties, which can make the electrons transmit across the Pt-2 film|Al interface easily. Based on the comprehensive consideration of EIS data, it can be prospected that the property of the Pt-2 CE is advantageous to improve the photovoltaic performance of the FFDSSCs.

Figure 6 presents the Tafel curves for the symmetrical cells similar to the ones used in the EIS measurements

Table 1 Cyclic voltammograms and EIS parameters of the various CEs

No.	CE	R_s ($\Omega\text{ cm}^2$)	R_{ct} ($\Omega\text{ cm}^2$)	Z_w ($\Omega\text{ cm}^2$)	$ E_{pp} $ (V)	$ j_{pc} $ (mA cm^{-2})
a	Pt	3.75	3.10	1.62	0.310	2.85
b	Pt-1	3.96	3.99	1.09	0.231	2.10
c	Pt-2	3.57	3.11	1.05	0.230	2.87



to reconfirm the electrocatalytic activity of the Pt-1, Pt-2, and pure Pt CEs. As seen in Fig. 6, the Pt-2 CE shows much larger exchange current density (J_0) and limiting diffusion current density (J_{lim}) (1.48 and 2.18 mA cm⁻²) in comparison with that of the Pt-1 CE (1.28 and 1.89 mA cm⁻²), suggesting higher conductivity and electrocatalytic ability for the Pt-2 CE. Also, the higher J_{lim} for the Pt-2 CE reflects faster diffusion velocity for the redox couple in the electrolyte [23–25]. Additionally, as expected, the electrocatalytic activity of the Pt-2 CE is shown as excellent as the pure Pt CE. These positive factors can be attributed to the same reasons as CV and EIS, which logically result in an efficient power conversion efficiency for the FFDSSC. In theory, J_0 is inversely proportional to R_{ct} according to Eq. (5) [26, 27]. The changed tendency of J_0 in Tafel curves for the Pt-1, Pt-2, and pure Pt CEs is generally in accordance with the EIS. Generally,

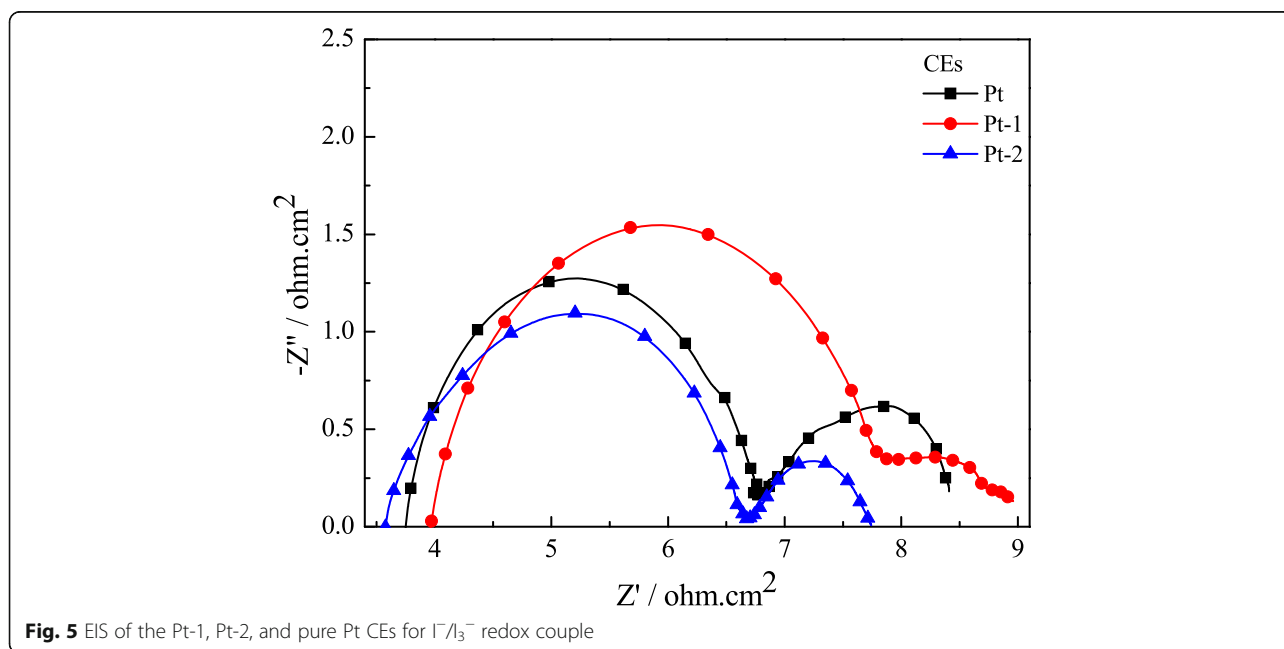
the extensive electrochemical measurements results (CVs, EIS, and Tafel) indicate that the Pt-2 CE possesses an enhanced electrocatalytic activity compared to that of the pure Pt CE; thus, it can be logically expected a considerable improvement in the photovoltaic performance for the FFDSSC.

$$J_0 = \frac{RT}{nFR_{ct}} \tag{5}$$

where R is the gas constant, T , F , n , and R_{ct} have their usual meaning.

Photovoltaic performance of the FFDSSCs

J-V characteristics of the FFDSSCs with different CEs and photoanodes were measured under 100 mW cm⁻²



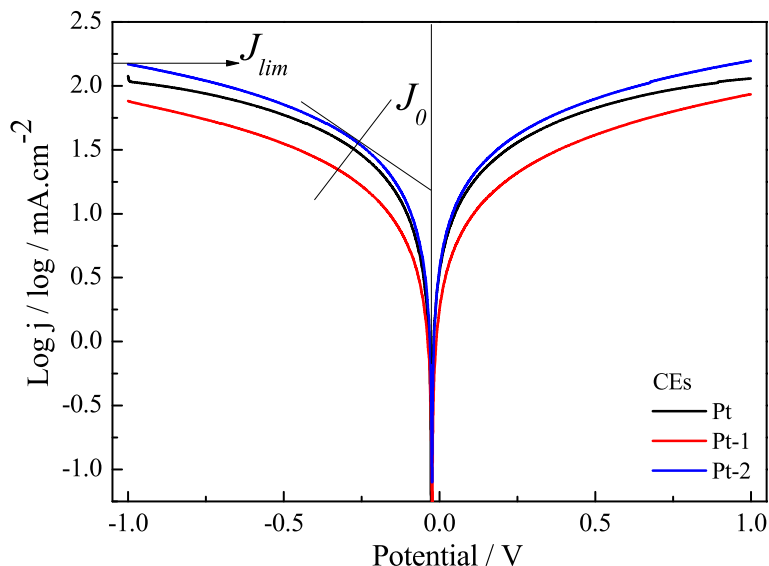


Fig. 6 Tafel curves of the symmetrical Pt-1, Pt-2, and pure Pt CEs for I_3^-/I^- redox couple

(AM 1.5 G) irradiation, and the results are presented in Fig. 7 and Table 2. Curves b and c present the FFDSSCs assembled with Pt-1 and Pt-2 CEs and TiO_2 photoanode without $TiCl_4$ modified in Fig. 7, which are not smooth. However, it is important to note that the open-circuit voltage (V_{oc}) and short-circuit current density (J_{sc}) of the FFDSSC-c (0.760 V and 10.78 mA cm^{-2}) is much higher than that of the FFDSSC-b (0.625 V and 10.78 mA cm^{-2}). This phenomenon is associated with the low R_{ct} , excellent electrochemical catalytic activity and conductivity for the Pt-2 CE, and the increased contact area between the Pt-2 CE and the electrolyte [28, 29]. Curves d and e of the FFDSSCs with Pt-1 and Pt-2 CEs and TiO_2 photoanode with $TiCl_4$ modified display the smooth curves with high V_{oc} , J_{sc} , and fill factor (FF). Between them, the higher photoelectric performance for the FFDSSC-e is mainly

originating from the lower R_{ct} and more excellent electrochemical catalytic activity and conductivity for the Pt-2 CE compared to that of the FFDSSC-a based on the pure Pt CE and TiO_2 photoanode with $TiCl_4$ modified (6.32%). Additionally, the more important reasons are attributed to the $TiCl_4$ modification, which increases the photoelectrons generated rate by the excited dye molecules and reduces the recombination rate of the electron and Ti wire; thus, the device logically shows better V_{oc} , J_{sc} , and FF values. Conversely, the FFDSSC based on the TiO_2 photoanode without modification by the $TiCl_4$ shows a worse photovoltaic performance. Simultaneously, the twice modification for the CE significantly influences on the performance of FFDSSC, which increases the electrolyte loading on the CE surface, and decreases the internal resistance and dark current of the FFDSSC, thus

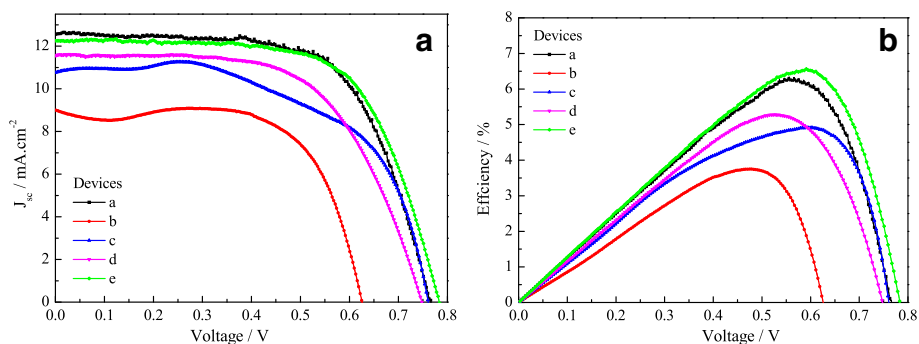


Fig. 7 Photovoltaic performance curves for the FFDSSCs fabricated with various photoanodes and the CEs under the standard illumination. J-V characteristics of the FFDSSCs (a); the relationship between power conversion efficiency and the open-circuit voltage (b)

Table 2 The photocurrent-voltage parameters of the FFDSSCs assembled with various photoanodes and the counter electrodes

No.	CEs	Photoanodes	V_{oc} (V)	J_{sc} (mA cm^{-2})	FF	η (%)
a	Pt	TiCl ₄ modified	0.766	12.55	0.657	6.32
b	Pt-1	without TiCl ₄	0.625	8.98	0.667	3.74
c	Pt-2	without TiCl ₄	0.760	10.78	0.602	4.93
d	Pt-1	TiCl ₄ modified	0.747	11.59	0.611	5.29
e	Pt-2	TiCl ₄ modified	0.783	12.25	0.662	6.35

greatly improving the J_{sc} values. These indicate that the twice modifications for the electrode facilitate fast electron transport at the interface between I^-/I_3^- electrolyte and the electrodes, and it also can be deduced that the FFDSSC based on the Pt-2 CE and TiO₂ photoanodes modified with TiCl₄ can indeed improve the charge recombination and have a more outstanding effect than other FFDSSCs.

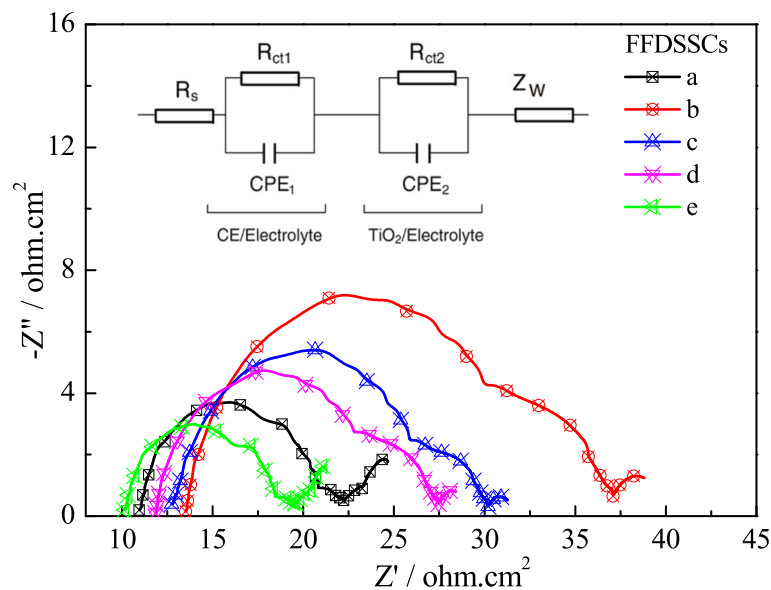
Figure 8 shows the Nyquist plots of the FFDSSCs based on different CEs and photoanodes under 100 mW cm^{-2} (AM 1.5 G) irradiation, and the equivalent circuit is shown as the inset. R_s is the series resistance, and R_{ct} is the charge transfer resistance at the interface of electrolyte/photoanode. R_s and R_{ct} values for the FFDSSCs with compact layer made from TiCl₄ modified (FFDSSCs a, d, e) are lower than those of the FFDSSCs without TiCl₄ modified; this is due to the ultrathin TiO₂ compact layer with a high electron mobility enhanced the interface contact between Ti wire and TiO₂ photoanode, and it also reduces the probability of electron recombination [30, 31]. Furthermore, the FFDSSC-e possesses the smallest R_s and

R_{ct} values among the FFDSSCs a, d, and e, which is smaller than that of the FFDSSC-a. This indicates that the Pt-2 CE with twice modifications in the FFDSSC is more beneficial to electron transport at the interface between I^-/I_3^- electrolyte and the electrodes than that of the pure Pt CE. As a consequence, the multiple modifications for the anode and counter electrode in FFDSSCs are conducive to improve the photovoltaic performance.

Figure 9 displays the IPCE of the FFDSSCs with different CEs and photoanodes to reflect the light response, which is directly related to J_{sc} . As shown in Fig. 9, the maximum efficiency of all the FFDSSCs at the wavelength of about 520 nm is in coincidence with the absorption maximum wavelength of dye N719 [32, 33]. IPCE maximum peak for the above mentioned FFDSSCs follows the orders of $e > a > d > c > b$. This result is in good agreement with the photovoltaic performances as shown in Fig. 7, which also proves again that the multiple modifications for the anode and counter electrode can remarkably improve the photoelectric performance for the FFDSSCs.

Conclusions

An efficient flexible fibrous dye-sensitized solar cell (FFDSSC) was fabricated with a multilayer-structure fibers TiO₂ photoanode (modified with TiCl₄) and a Pt-2 CE with double-layer structure to improve the performance of the device. Pt-2 fiber CE demonstrates excellent electrocatalytic activity for the reduction of triiodide in FFDSSC through the cyclic voltammetry, electrochemical impedance spectroscopy, and Tafel characterization. The FFDSSC based on the Pt-2 fiber electrode and TiO₂ fiber photoanode modified with TiCl₄ shows a

**Fig. 8** EIS for the FFDSSCs fabricated with the various photoanodes and the CEs under the standard illumination

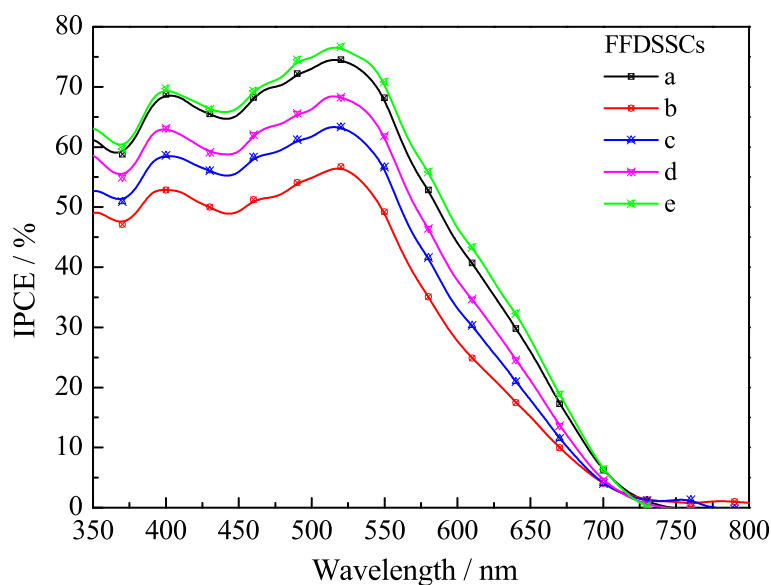


Fig. 9 The IPCE of the various FFDSSCs

photoelectric conversion efficiency of 6.35%, 69.8% higher than that of with monolayer fiber TiO_2 photoanode and electrodeposition of Pt wire, which is comparable to that of the FFDSSC based on the pure Pt wire CE. This low-cost and easy fabrication FFDSSC with high elasticity, flexibility, and stretchability could prepare high-performance wearable micro-solar cells to adapt to complex mechanical deformations, which have vast potential to develop a new family in energy conversion and storage devices.

Abbreviations

CE: Counter electrode; CV: Cyclic voltammetry; FFDSSC: Flexible fibrous dye-sensitized solar cell; Γ^-/I_3^- : Iodide/triiodide; J_0 : Exchange current density; J_{lim} : Limiting current density; J_{max} : Maximum current density; J_{sc} : Short-circuit current density; J-V: Photocurrent-photovoltage; PCE: Power conversion efficiency; P_{in} : Incident light power; R_{ct} : Charge transfer resistance; R_s : Series resistance; SEM: Scanning electron microscopy; V_{max} : Maximum voltage; V_{oc} : Open-circuit voltage

Acknowledgements

The authors are very grateful to the joint support by NSFC (No. U1504624, 61704047, U 1404619, and 51372069). This work is also supported by Science and Technology Development Project of Henan Province (132300410142, 152300410060).

Authors' contributions

GY carried out the experiments, participated in the sequence alignment, and drafted the manuscript. XL participated in the device preparation. JH was involved in the SEM, EIS, and CV analysis of the devices. YC and HZ helped to draft the manuscript. All authors read and approved the final manuscript.

Competing interests

The authors declare that they have no competing interests.

Publisher's Note

Springer Nature remains neutral with regard to jurisdictional claims in published maps and institutional affiliations.

Author details

¹Henan Key Laboratory of Photovoltaic Materials, Henan University, Kaifeng 475004, China. ²School of Physics & Electronics, Henan University, Kaifeng 475004, China. ³School of Materials Science and Engineering, Shaanxi University of Science and Technology, Xi'an 710021, China.

Received: 26 March 2018 Accepted: 13 June 2018

Published online: 28 June 2018

References

- O'Regan B, Grätzel M (1991) A low-cost, high-efficiency solar cell based on dye-sensitized colloidal TiO_2 films. *Nature* 353:737–740
- Yella A, Lee HW, Tsao HN, Yi CY, Chandiran AK, Nazeeruddin MK, Diau EWG, Yeh CY, Zakeeruddin SM, Grätzel M (2011) Porphyrin-sensitized solar cells with cobalt (II/III)-based redox electrolyte exceed 12 percent efficiency. *Science* 334:629–634
- Hou S, Cai X, Fu Y, Lv Z, Wang D, Wu H, Zhang C, Chu Z, Zou D (2011) Transparent conductive oxide-less, flexible, and highly efficient dye-sensitized solar cells with commercialized carbon fiber as the counter electrode. *J Mater Chem* 21:13776–13779
- Sun H, Deng J, Qiu L, Fang X, Peng H (2015) Recent progress in solar cells based on one-dimensional nanomaterials. *Energy Environ Sci* 8:1139–1159
- Fu X, Sun H, Xie S, Zhang J, Pan Z, Liao M, Xu L, Li Z, Wang B, Sun X, Peng H (2018) A fiber-shaped solar cell showing a record power conversion efficiency of 10%. *J Mater Chem A* 6:45–51
- Peng M, Zou D (2015) Flexible fiber/wire-shaped solar cells in progress: properties, materials, and designs. *J Mater Chem A* 3:20435–20458
- Sun H, Yang Z, Chen X, Qiu L, You X, Chen P, Peng H (2013) Photovoltaic wire with high efficiency attached onto and detached from a substrate using a magnetic field. *Angew Chem Int Ed* 52:8276–8280
- Sun H, You X, Deng J, Chen X, Yang Z, Chen P, Fang X, Peng H (2014) A twisted wire-shaped dual-function energy device for photoelectric conversion and electrochemical storage. *Angew Chem Int Ed* 53:6664–6668
- Ali A, Shehzad K, Ur-Rahman F, Shah SM, Khurram M, Mumtaz M, Sagar RUR (2016) Flexible, low cost, and platinum-free counter electrode for efficient dye-sensitized solar cells. *ACS Appl Mater Interfaces* 8:25353–25360
- Chen T, Qiu L, Yang Z, Peng H (2013) Novel solar cells in a wire format. *Chem Soc Rev* 42:5031–5041
- Yue GT, Wu JH, Xiao YM, Huang ML, Lin JM, Fan LQ, Lan Z (2013) Platinum/graphene hybrid film as a novel counter electrode for dye-sensitized solar cells. *Electrochim Acta* 92:64–70

12. Papergiou N (2004) Counter-electrode function in nanocrystalline photoelectrochemical cell configurations. *Coord Chem Rev* 248:1421–1446
13. Murakami TN, Grätzel M (2008) Counter electrodes for DSC: application of functional materials as catalysts. *Inorg Chim Acta* 361:572–580
14. Chen C, Chen C, Wei T (2010) Chemical deposition of platinum on metallic sheets as counter electrodes for dye-sensitized solar cells. *Electrochim Acta* 55:1687–1695
15. Yue GT, Ma XP, Jiang QW, Tan FR, Wu JH, Chen C, Li FM, Li QH (2014) PEDOT:PSS and glucose assisted preparation of molybdenum disulfide/single-wall carbon nanotubes counter electrode and served in dye-sensitized solar cells. *Electrochim Acta* 142:68–75
16. Yue GT, Wang L, Zhang XA, Wu JH, Jiang QW, Zhang WF, Huang ML, Lin JM (2014) Fabrication of high performance multi-walled carbon nanotubes/polypyrrole counter electrode for dye-sensitized solar cells. *Energy* 67:460–467
17. Liu XQ, Liang Y, Yue GT, Tu YG, Zheng HW (2017) A dual function of high efficiency quasi-solid-state flexible dye-sensitized solar cell based on conductive polymer integrated into poly (acrylic acid-co-carbon nanotubes) gel electrolyte. *Sol Energy* 148:63–69
18. Tang ZY, Wu JH, Zheng M, Huo JH, Lan Z (2013) A microporous platinum counter electrode used in dye-sensitized solar cells. *Nano Energy* 2:622–627
19. Yue GT, Wu JH, Xiao YM, Huang ML, Lin JM, Lin J-Y (2013) High performance platinum-free counter electrode of molybdenum sulfide-carbon used in dye-sensitized solar cells. *J Mater Chem A* 1:1495–1501
20. Sun H, Luo Y, Zhang Y, Li D, Yu Z, Li K, Meng Q (2010) In situ preparation of a flexible polyaniline/carbon composite counter electrode and its application in dye-sensitized solar cells. *J Phys Chem C* 114:11673–11679
21. Jang YH, Rani A, Quan LN, Adinolfi V, Kanjanaboos P, Ouellette O, Son T, Jang YJ, Chung K, Kwon H, Kim D, Kim DH, Sargent EH (2017) Graphene oxide shells on plasmonic nanostructures lead to high-performance photovoltaics: a model study based on dye-sensitized solar cells. *ACS Energy Lett* 2:117–123
22. Cui Y, Zhang L, Lv K, Zhou G, Wang Z-S (2015) Low temperature preparation of TiO₂ nanoparticle chains without hydrothermal treatment for highly efficient dye-sensitized solar cells. *J Mater Chem A* 3:4477–4483
23. Zakeeruddin SM, Grätzel M (2009) Solvent-free ionic liquid electrolytes for mesoscopic dye-sensitized solar cells. *Adv Funct Mater* 19:2187–2202
24. Liu L, Yoo SH, Park S (2010) Synthesis of vertically aligned hollow platinum nanotubes with single crystalline nanoflakes. *Chem Mater* 22:2681–2684
25. Yue GT, Wu W, Liu XQ, Zheng HW (2018) Enhanced Photovoltaic Performance of Dye-Sensitized Solar Cells based on a Promising Hybrid Counter Electrode of CoSe₂/MWCNTs. *Sol. Energy* 167:137–146
26. Yue GT, Wu JH, Lin J-Y, Xiao YM, Lin JM, Huang ML, Lan Z (2013) A counter electrode of multi-wall carbon nanotubes decorated with tungsten sulfide used in dye-sensitized solar cells. *Carbon* 55:1–9
27. Wu MX, Lin X, Wang TH, Qiu JS, Ma TL (2011) Low-cost dye-sensitized solar cell based on nine kinds of carbon counter electrodes. *Energy Environ Sci* 4: 2308–2315
28. Ri JH, Wu SF, Jin JP, Peng TY (2017) Growth of sea urchin-like rutile TiO₂ hierarchical microspheres film on Ti foil for quasi-solid-state dye-sensitized solar cell. *Nanoscale* 9:18498–18506
29. Lu S, Wang YL, Li F, Yang GC, Yang HY, Zhang XT, Liu YC (2017) Adsorption energy optimization of Co₃O₄ through rapid surface sulfurization for efficient counter electrode in dye-sensitized solar cells. *J Phys Chem C* 121: 12524–12530
30. Ke W, Fang G, Liu Q, Xiong L, Qin P, Tao H, Wang J, Lei H, Li B, Wan J, Yang G, Yan Y (2015) Low-temperature solution-processed tin oxide as an alternative electron transporting layer for efficient perovskite solar cells. *J Am Chem Soc* 137:6730–6733
31. Liu Q, Qin M, Ke W, Zheng X, Chen Z, Qin P, Xiong L, Lei H, Wan J, Wen J, Yang G, Ma J, Zhang Z, Fang G (2016) Enhanced stability of perovskite solar cells with low-temperature hydrothermally grown SnO₂ electron transport layers. *Adv Funct Mater* 26:6069–6075
32. Wang Z, Kawauchi H, Kashima T, Arakawa H (2004) Significant influence of TiO₂ photoelectrode morphology on the energy conversion efficiency of N719 dye-sensitized solar cell. *Coord Chem Rev* 248:1381–1389
33. Yue JY, Xiao YM, Li YP, Han GY, Zhang YY, Hou WJ (2017) Enhanced photovoltaic performances of the dye-sensitized solar cell, by utilizing rare-earth modified tin oxide compact layer. *Org Electron* 43:121–129

Submit your manuscript to a SpringerOpen® journal and benefit from:

- Convenient online submission
- Rigorous peer review
- Open access: articles freely available online
- High visibility within the field
- Retaining the copyright to your article

Submit your next manuscript at ► springeropen.com